UKACC International Conference on Control 2012
Cardiff, UK, 3-5 September 2012

Path following for small UAVs in the presence of wind disturbance

Cunjia Liu* Owen McAree† and Wen-Hua Chen‡
Department of Aeronautical and Automotive Engineering
Loughborough University, Lecistershire, UK. LE11 3TU
Email: *c.liu5@lboro.ac.uk †o.mcaree@lboro.ac.uk ‡w.chen@lboro.ac.uk

***Abstract*—This paper presents an alternative approach of designing a guidance controller for a small Unmanned Aerial Vehicle (UAV) to achieve path following in the presence of wind disturbances. The wind effects acting on the UAV are estimated by a nonlinear disturbance observer. Then the wind information is incorporated into the nominal path following controller to formulate a composite controller so as to compensate wind influences. The globally asymptotic stability of the composite controller is illustrated through theoretical analysis and its performance is evaluated by various simulations including the software-in-the-loop. Initial flight tests using a small aircraft are carried out to demonstrate its actual performance.**

I. Introduction

The application of Unmanned Aerial Vehicles (UAVs) has been found in various areas not limited to military operations, but also in civil areas such as aerial photography and precision agriculture. Most of the UAV operations essentially are composed of commanding UAVs to fly through a series of spatial locations or paths either with or without a temporal requirement. This requirement categories flight patterns into two types, namely the trajectory tracking and path following [1]. The former suggests that the UAV needs to be in a particular position at a prespecified time, whereas the latter requires the UAV to converge to a geometric path with any feasible speed profile. In this paper, the path following problem is considered because it is less likely to push UAVs to their performance limits [2]. Moreover, with the influences of wind disturbance the trajectory tracking ability of an UAV can be easily compromised, which leaves the path following as an effective way to execute a task.

Path following as one of the motion control problems has been extensively studied especially for wheeled robots. In the field of UAV application, although vehicle dynamics are more complicated, the most recent micro aircraft are equipped with autopilots that provide the inner-loop stabilisation. For example, the UAV used in this study is installed with an Ardupilot autopilot which implements three PID controllers to achieve altitude-hold and airspeed-hold using elevator and throttle and the coordinated turn using aileron and rudder, which endows the UAV the ability to track the heading rate demand from the guidance controller. This means that the outloop behaviour of the UAV in level flight can be abstracted at a kinematic level by using a unicycle model. To this end, this paper adopts a path following method stemmed from wheeled robots [3], which has since been extended to 3-D case for UAV applications [4]. But the main purpose of this study is to improve path following accuracy under wind conditions.

In terms of the micro fixed-wing aircraft considered in this paper, their light structure and limited power allows wind disturbances to have a strong effect on them. A common strategy to eliminate the influence of wind on path following is to overlook the airspeed of an UAV and focus on the its ground track [5], [6]. In this case, the ground velocity and flight course are required in the feedback signals. This information can be calculated from GPS position by differentiation or more elaborately can be provided by an onboard inertial navigation system (INS). However, for a micro UAV equipped with a low-cost sensor suit, these flight data may be not of good quality, whereas the fast dynamics of small vehicles are highly susceptible to the low rate and delay of the GPS feedback signal. It is therefore more convenient to use the smooth airspeed measurement, magnetic heading and original GPS position data to realise the guidance function.

Another approach to solve wind effects on an UAV is to explicitly take them into account in path planning or control algorithms [7]–[9]. The knowledge of wind conditions is therefore required in such applications. Following on this direction, this paper adopts an alternative approach that exploits the use of a nonlinear disturbance observer [10]. The disturbance observer is designed to provide the estimates of external wind, which are then incorporated into the nominal path following controller. This results in a composite controller for UAV path following. Note that the wind disturbances are assumed to be near constant in the analysis because only these components cause a steady state error. However, the ability of estimating the varying wind are also demonstrated in the simulation section. In addition, the disturbance observer can provide estimates of disturbances other than wind gust such as aircraft trimming errors, which cause the system to behave differently from the nominal model [11].

The composite controller comprising the disturbance observer and the nonlinear guidance law is shown to be globally asymptotically stable by using the control theory on cascaded systems [12]. This suggests that the proposed control system can guarantee the path following accuracy in spite of wind disturbances. The performance of the proposed controller is demonstrated in the simulations as well as in real flight experiments using our newly developed flight test platform.

978-1-4673-1558-6/12/$31.00 ©2012 IEEE

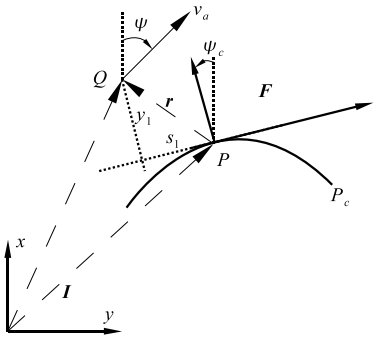

Fig. 1. Frame configuration

II. Problem formulation

The problem considered in this paper is the accurate path following for UAVs in the presence of wind. The objective of path following is to guide the UAV to converge to a desired geometric path described by some parameters, e.g. the path length. When wind disturbances are introduced to the system, necessary actions need to be taken to prevent their effects on the path following performance.

The kinematics of a fixed-wing UAV can be described using the following unicycle model under the assumptions that the UAV is in level flight with a near constant air speed:

$$\begin{aligned} \dot{x} &= v_a \cos(\psi) + w_x \\ \dot{y} &= v_a \sin(\psi) + w_y \\ \dot{\psi} &= \omega \end{aligned} \tag{1}$$

where (x, y) is the position of the UAV in the inertial frame $\mathcal{I}$, ψ is the UAV heading angle, v_a is the airspeed, (w_x, w_y) is the velocity of the wind disturbance in x and y directions, respectively, and ω is the heading rate. By constructing a control input ω, the position output should be able to follow a prescribed path $P_c(s) = \begin{bmatrix} x_c(s) & y_c(s) \end{bmatrix}^T$, which is a spatial curve and parameterised by its length s.

The path following function can be achieved by controlling the UAV to follow a virtual target running along the target path [3], [4]. To this end, it is natural to present the generalised error between the UAV and the virtual target in a moving frame attached to this virtual target. In the inertial frame $\mathcal{I}$, let Q be the UAV position and P denote the point on the path $P_c(s)$ to be followed, i.e. the virtual target. A Serret-Frenet frame $\mathcal{F}$ can be established on the point P as shown in Fig.1, where the signed curvilinear abscissa is the path length s. Then, the UAV position Q can be expressed in the frame $\mathcal{I}$ as a vector $\boldsymbol{q} = \begin{bmatrix} x & y \end{bmatrix}^T$ and in the frame $\mathcal{F}$ as a vector $\boldsymbol{r} = \begin{bmatrix} s_1 & y_1 \end{bmatrix}^T$. Note that $\boldsymbol{r} = \boldsymbol{q} - \boldsymbol{p}$ is also the error vector, where $\boldsymbol{p}$ denotes the position vector of P in $\mathcal{I}$.

To minimise the error vector $\boldsymbol{r}$, its dynamics in frame $\mathcal{F}$ need to be investigated. First, by defining the heading rate of the desired path $\dot{\psi}_c = \omega_c$, we have the following relations:

$$\begin{aligned} \dot{\psi}_c &= \omega_c = c_c(s)\dot{s} \\ \dot{c}_c(s) &= g_c(s)\dot{s} \end{aligned} \tag{2}$$

where $c_c(s)$ and $g_c(s) = \frac{dc_c(s)}{ds}$ are the path curvature and its derivative, respectively. Next, the velocity of P in $\mathcal{I}$ can be expressed in frame $\mathcal{F}$, such that:

$$\left(\frac{d\boldsymbol{p}}{dt}\right)_F = \begin{bmatrix} \dot{s} & 0 \end{bmatrix}^T \tag{3}$$

For the position $\boldsymbol{q}$ of the UAV, its inertial velocity can be expressed in a moving frame such that:

$$\left(\frac{d\boldsymbol{q}}{dt}\right)_I = \left(\frac{d\boldsymbol{p}}{dt}\right)_I + R_F^I \left(\frac{d\boldsymbol{r}}{dt}\right)_F + R_F^I(\omega_c \times \boldsymbol{r}) \tag{4}$$

where $\times$ denotes the vector cross-product and R_F^I is the rotation matrix from frame $\mathcal{F}$ to $\mathcal{I}$. Left multiplying its inverse R_I^F on both side of (4) yields

$$R_I^F \left(\frac{d\boldsymbol{q}}{dt}\right)_I = \left(\frac{d\boldsymbol{p}}{dt}\right)_F + \left(\frac{d\boldsymbol{r}}{dt}\right)_F + \omega_c \times \boldsymbol{r} \tag{5}$$

Using the relations

$$\begin{aligned} \left(\frac{d\boldsymbol{q}}{dt}\right)_I &= \begin{bmatrix} \dot{x} & \dot{y} \end{bmatrix}^T \\ \left(\frac{d\boldsymbol{r}}{dt}\right)_F &= \begin{bmatrix} \dot{s}_1 & \dot{y}_1 \end{bmatrix}^T \end{aligned} \tag{6}$$

and the expansion of $\omega_c \times \boldsymbol{r}$, (5) can be rewritten as

$$R_I^F \begin{bmatrix} \dot{x} \\ \dot{y} \end{bmatrix} = \begin{bmatrix} \dot{s}(1 - c_c(s)y_1) + \dot{s}_1 \\ \dot{y}_1 + c_c(s)\dot{s}s_1 \end{bmatrix} \tag{7}$$

Solving (7) for $\dot{s}_1$ and $\dot{y}_1$ and combining (1) yields the dynamics of the path following error in the frame $\mathcal{F}$ at the kinematics level:

$$\begin{aligned} \dot{s}_1 &= -\dot{s}(1 - c_c y_1) + v_a \cos(\psi_e) + w_{f_x} \\ \dot{y}_1 &= -c_c \dot{s} s_1 + v_a \sin(\psi_e) + w_{f_y} \\ \dot{\psi}_e &= \omega - c_c \dot{s} \end{aligned} \tag{8}$$

where $\psi_e = \psi - \psi_c$ is the heading error,

$$\begin{aligned} w_{f_x} &= \cos\psi_c w_x + \sin\psi_c w_y \\ w_{f_y} &= -\sin\psi_c w_x + \cos\psi_c w_y \end{aligned} \tag{9}$$

are wind disturbances expressed in the frame $\mathcal{F}$, respectively. The designed path following controller needs to regulate this system to eliminate the state error under the wind disturbances.

It is intuitive to work out that if the wind elements are known, the aircraft can fly into wind with certain trim angle so that the projection of forward speed normal to the track can be used to cancel the wind effect. This basic idea provides the guideline for the designing our path following controller.

III. Disturbance observer based control

To obtain the estimates of wind disturbances, a nonlinear disturbance observer is first designed. This information is then incorporated into controller design. This design methodology is known as the disturbance observer based control (DOBC) [10].

A. Disturbance observer design

The UAV kinematic model (1) can be cast into a compact mode:

$$\dot{\boldsymbol{x}} = f(\boldsymbol{x}) + g_1(\boldsymbol{x})\boldsymbol{u} + g_2(\boldsymbol{x})\boldsymbol{d} \tag{10}$$

where state $\boldsymbol{x} = [\ x \quad y \quad \psi\ ]^T$, control input $\boldsymbol{u} = \omega$ and disturbance $\boldsymbol{d} = [\ w_x \quad w_y\ ]^T$. The system functions $f(\boldsymbol{x})$, $g_1(\boldsymbol{x})$ and $g_2(\boldsymbol{x})$ are derived from (1), such that:

$$f(\boldsymbol{x}) = \begin{bmatrix} v_a \sin\psi \\ v_a \cos\psi \\ 0 \end{bmatrix}, \quad g_1(\boldsymbol{x}) = \begin{bmatrix} 0 \\ 0 \\ 1 \end{bmatrix}, \quad g_2(\boldsymbol{x}) = \begin{bmatrix} 1 & 0 \\ 0 & 1 \\ 0 & 0 \end{bmatrix} \tag{11}$$

A disturbance observer is adopted to estimate w_x and w_y under the assumption that they are near constant, i.e. $\dot{w}_x \approx 0$ and $\dot{w}_y \approx 0$. The disturbance observer follows the standard design [10]:

$$\begin{aligned} \hat{\boldsymbol{d}} &= \boldsymbol{z} + p(\boldsymbol{x}) \\ \dot{\boldsymbol{z}} &= -l(\boldsymbol{x})g_2(\boldsymbol{x})\boldsymbol{z} - l(\boldsymbol{x})(g_2(\boldsymbol{x})p(\boldsymbol{x}) + f(\boldsymbol{x}) + g_1(\boldsymbol{x})\boldsymbol{u}) \end{aligned} \tag{12}$$

where $\hat{\boldsymbol{d}} = [\ \hat{w}_x \quad \hat{w}_y\ ]^T$ is the estimate of wind disturbance, $\boldsymbol{z}$ is the internal state of the nonlinear observer, $p(\boldsymbol{x})$ is a nonlinear function to be designed, and $l(\boldsymbol{x})$ is the nonlinear observer gain given by

$$l(\boldsymbol{x}) = \frac{\partial p(\boldsymbol{x})}{\partial \boldsymbol{x}} \tag{13}$$

The estimation error in the above observer is defined as $\boldsymbol{e}_d = \boldsymbol{d} - \hat{\boldsymbol{d}} = [\ e_x \quad e_y\ ]^T$. Under the assumption that the disturbance is slowly varying compared to the observer dynamics and by combining (12)-(13) and the system function (10), it can be shown that the estimation error has the following property:

$$\dot{\boldsymbol{e}}_d = \dot{\boldsymbol{d}} - \dot{\hat{\boldsymbol{d}}} = -\dot{\boldsymbol{z}} - \frac{\partial p(\boldsymbol{x})}{\partial \boldsymbol{x}}\dot{\boldsymbol{x}} = -l(\boldsymbol{x})g_2(\boldsymbol{x})\boldsymbol{e}_d \tag{14}$$

Therefore, the observer design problem is converted to chose an appropriate observer gain $l(\boldsymbol{x})$ such that (14) is globally exponentially stable regardless of state $\boldsymbol{x}$.

In this paper, since the function g_2 is a constant matrix, the observer gain can be simply chosen as

$$l(\boldsymbol{x}) = \begin{bmatrix} l_x & 0 & 0 \\ 0 & l_y & 0 \end{bmatrix} \tag{15}$$

where l_x and l_y are positive constants to be tuned. Correspondingly, the nonlinear function $p(\boldsymbol{x})$ can be calculated by integrating $l(\boldsymbol{x})$ with respect to $\boldsymbol{x}$ based on (13).

B. Control synthesis

After the wind estimates are obtained, the next step is to design a path following controller that regulates the error system (8) to its origin. According to the design guideline, the UAV can fly into wind with a trimming angle ψ_0 so that the side component of the forward velocity neutralises the wind component that drives the UAV away from the desired path.

Given that the wind estimates are available, the estimated trimming angle can be written as $\psi_{\hat{0}} = -\sin^{-1}\frac{\hat{w}_{f_y}}{v_a}$. Furthermore, the error dynamics (8) can be reformulated to facilitate the control design:

$$\begin{aligned} \dot{s}_1 &= -\dot{s}(1 - c_c y_1) + v_a \cos(\psi_{\hat{w}} + \psi_{\hat{0}}) + \hat{w}_{f_x} + e_{f_x} \\ \dot{y}_1 &= -c_c \dot{s} s_1 + v_a \sin(\psi_{\hat{w}} + \psi_{\hat{0}}) + \hat{w}_{f_y} + e_{f_y} \\ \dot{\psi}_{\hat{w}} &= \omega - c_c \dot{s} - \dot{\psi}_{\hat{0}} \end{aligned} \tag{16}$$

where $\psi_{\hat{w}} = \psi_e - \psi_{\hat{0}}$, $\hat{w}_{f_x}$ and $\hat{w}_{f_y}$ are calculated from (9) after $\hat{w}_x$ and $\hat{w}_y$ are estimated in (12), such that $\hat{w}_{f_x} + e_{f_x} = w_{f_x}$, $\hat{w}_{f_y} + e_{f_y} = w_{f_y}$. Carrying out the differentiation of $\psi_{\hat{0}}$ with respect to time gives:

$$\begin{aligned} \dot{\psi}_{\hat{0}} = &\frac{1}{\sqrt{v_a^2 - \hat{w}_{f_y}^2}} \underbrace{(\cos\psi_c \hat{w}_x + \sin\psi_c \hat{w}_y)}_{\hat{w}_{f_x}} c_c \dot{s} + \\ &\frac{1}{\sqrt{v_a^2 - \hat{w}_{f_y}^2}} (\sin\psi_c l_x e_x - \cos\psi_c l_y e_y) \end{aligned} \tag{17}$$

where the relations $\dot{\hat{w}}_* = \dot{w}_* - \dot{e}_* = -\dot{e}_*$ and $\dot{e}_* = -l_* e_*$ are used while '$*$' denoting x and y. Moreover, one can define $\dot{\psi}_{\hat{0}} = \dot{\psi}_{\tilde{0}} + e_\psi$, where

$$\dot{\psi}_{\tilde{0}} = \frac{\hat{w}_{f_x}}{\sqrt{v_a^2 - \hat{w}_{f_y}^2}} c_c \dot{s} \tag{18}$$

and

$$e_\psi = \dot{\psi}_{\hat{0}} - \dot{\psi}_{\tilde{0}} = \frac{\sin\psi_c l_x e_x - \cos\psi_c l_y e_y}{\sqrt{v_a^2 - \hat{w}_{f_y}^2}} \tag{19}$$

At this stage, the problem of path following in the presence of wind can be solved by driving the states of system (16) to zero. This objective can be embodied in the Lyapunov function candidate:

$$V = \frac{1}{2}k_1 s_1^2 + \frac{1}{2}k_1 y_1^2 + \frac{1}{2}\psi_{\hat{w}}^2 \tag{20}$$

Its derivative can be calculated by invoking (16)-(19) as:

$$\begin{aligned} \dot{V} = &-k_1 s_1 (\dot{s} - v_a cos\psi_e - \hat{w}_{f_x} - e_{f_x}) \\ &+ k_1 y_1 (v_a \sin\psi_e + \hat{w}_{f_y} + e_{f_y}) \\ &+ \psi_{\hat{w}} (\omega - c_c \dot{s} - \dot{\psi}_{\tilde{0}} - e_\psi) \end{aligned} \tag{21}$$

where k_1 is a positive constant. In the observation of (21), a nonlinear control law is proposed for path following in conjunction with the disturbance observer (12):

$$\begin{aligned} \dot{s} &= k_2 s_1 + v_a \cos\psi_e + \hat{w}_{f_x} \\ \omega &= -k_3 \psi_{\hat{w}} - k_1 y_1 \frac{v_a \sin\psi_e + \hat{w}_{f_y}}{\psi_{\hat{w}}} + c_c(s)\dot{s} + \dot{\psi}_{\tilde{0}} \end{aligned} \tag{22}$$

where k_2 and k_3, together with k_1 are positive parameters to be tuned in the controller. It also can be shown that:

$$\lim_{\psi_{\hat{w}} \to 0} \frac{v_a \sin\psi_e + \hat{w}_{f_y}}{\psi_{\hat{w}}} = v_a \cos(\frac{\psi_e + \psi_{\hat{0}}}{2}) \tag{23}$$

The closed-loop stability under the composite controller needs to be investigated. In the following, we will first show the stability with no estimation error, and the stability with the disturbance observer.

Proposition 1: Given the estimation error $\boldsymbol{e}_d = 0$, i.e. the exact wind knowledge is available, the time-varying system (16) under the control of (22) is globally asymptotically stable.

Proof: Consider the Lyapunov function candidate (20). Substituting (22) into its time derivative (21) and using the assumption that $\boldsymbol{e}_d = 0$ gives:

$$\dot{V} = -k_1 k_2 s_1^2 - k_3 \psi_{\hat{w}}^2 \leq 0 \tag{24}$$

Thus, V is non-increasing, and this implies the states s_1, y_1 and $\psi_{\hat{w}}$ are bounded and V converges to some limited value. According to Barbalat's Lemma, $\dot{V}$ converges to zero since it is uniformly continuous. From the observation of (24), s_1 and $\psi_{\hat{w}}$ asymptotically converge to zero.

Furthermore, by inserting the control law (22) into the system (16), it can be found that

$$\dot{\psi}_{\hat{w}} = -k_3 \psi_{\hat{w}} - k_1 y_1 \frac{v_a \sin\psi_e + \hat{w}_{f_y}}{\psi_{\hat{w}}} \tag{25}$$

As $\psi_{\hat{w}}$ approaches zero, $\dot{\psi}_{\hat{w}}$ also tends to zeros according to Barbalat's lemma. Because $\frac{v_a \sin\psi_e + \hat{w}_{f_y}}{\psi_{\hat{w}}} \neq 0$, y_1 is shown to converge to zero. ■

However, in practice the exact wind information is unknown, and its estimates are provided by the disturbance observer. Although the estimation error converges to zero regardless of the system states, the transit period still needs to be investigated. Thus, the stability of the overall system needs to take into account the observer dynamics. Such a system can be considered as a cascaded time-varying system:

$$\dot{\boldsymbol{x}}_1 = f_1(t, \boldsymbol{x}_1) + h(t, \boldsymbol{x}_1, \boldsymbol{x}_2)\boldsymbol{x}_2 \tag{26a}$$

$$\dot{\boldsymbol{x}}_2 = f_2(t, \boldsymbol{x}_2) \tag{26b}$$

where $\boldsymbol{x}_1 = [\ s_1 \quad y_1 \quad \psi_{\hat{w}}\ ]^T$ and $\boldsymbol{x}_2 = [\ e_x \quad e_y\ ]^T$. The upper system corresponds to the system (16) and the lower system is (14), where function f_1 and f_2 represent the corresponding terms in these equations, respectively. The function $h(t, \boldsymbol{x}_1, \boldsymbol{x}_2)$ can be explicitly written as

$$h(t, \boldsymbol{x}_1, \boldsymbol{x}_2) = \begin{bmatrix} \cos\psi_c & \sin\psi_c \\ -\sin\psi_c & \cos\psi_c \\ \frac{-\sin\psi_c l_x}{\sqrt{v_a^2 - \hat{w}_{f_y}^2}} & \frac{\cos\psi_c l_y}{\sqrt{v_a^2 - \hat{w}_{f_y}^2}} \end{bmatrix} \tag{27}$$

This cascaded system can be examined by using the Theorems in [12], from which the following lemma can be drawn:

Lemma 2: [12] Consider the cascaded system (26). Assume that the upper system is globally uniformly asymptotically stable with a Lyapunov function of the form $V(t, \boldsymbol{x}) = k\|\boldsymbol{x}\|^p$, for all $k > 0$ and $p > 1$, whose derivative only needs to be negative-semi-definite and the lower system is global exponentially stable. If the function $h(t, \boldsymbol{x}_1, \boldsymbol{x}_2)$ satisfies

$$\|h(t, \boldsymbol{x}_1, \boldsymbol{x}_2)\| \leq \theta_1(\|\boldsymbol{x}_2\|) + \theta_2(\|\boldsymbol{x}_2\|)\|\boldsymbol{x}_1\| \tag{28}$$

where θ_1 and θ_2 are continuous, then the cascaded system is globally uniformly asymptotically stable.

Theorem 3: Assume the wind disturbances are bounded and smaller than the airspeed $v_a > 0$, the error dynamics (16) of the path following problem is globally uniformly asymptotically stable under the control of the composite control law (22) and (12).

Proof: The proof follows the Lemma 2 to verify all the assumptions in it. First, from Proposition 1, the upper system is globally uniformly asymptotically stable and the Lyapunov function (20) satisfies the related assumptions. Then, the lower system is exponentially stable by choosing the observer gain according to (15). At last, the function $\|h(t, \boldsymbol{x}_1, \boldsymbol{x}_2)\| \leq (2 + \frac{l_x^2 + l_y^2}{v_a})^{\frac{1}{2}}$ from its definition. ■

IV. Simulations and Experiments

A. Simulation results

The proposed path following controller based on the disturbance observer was first verified in simulation. A comparison test is presented here to compare it with the nominal controller without wind correction and two PID-like controllers based on the cross-track error [13] and the cross-track angle [14], respectively. In this test, the desired path is composed of line segments connecting four waypoints. The UAV was flying at a low airspeed of 5m/s with the wind condition $w_x = 1.5$m/s and $w_y = 2$m/s, and the yaw rate is saturated at 0.5rad/s.

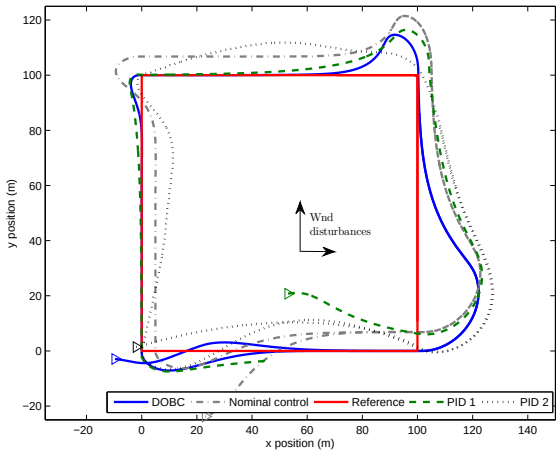

Fig. 2. Simulation Results

The simulation results are given in Fig.2. It can be seen that the proposed controller outperforms the others in terms of the path following accuracy, although the wind speed is 50% of the airspeed. The nominal controller without wind correction is able to follow the path but with steady state error due to the wind. The first PID controller based on the cross-track error can provide a competitive result but it suffers practical issues because noisy feedback signals [13]. The second PID control is based on the cross-track angle so that it aims at the next waypoint and converges to the path slowly. Note that all the controllers exhibit large converging errors at the lower right corner. This is because that the UAV heading deviated towards negative y direction before the corner and need to fly into wind

towards negative x direction after the corner, so that a large heading change is experienced during the turning.

B. Software-in-the-loop test

Before applying this new algorithm on the real UAV, more realistic tests need to be carried out to further evaluate its performance and minimise the risk in flight experiment. The software-in-the-loop (SIL) test is therefore performed to bridge up the gap between the numerical simulation and the practical experiment.

The structure of the SIL used in this study is shown in Fig 3. The test environment comprises three main components, namely the proposed algorithm to be tested, the Ardupilot code for the inner-loop stabilisation and the UAV dynamic model with a flight environment. The path following controller is implemented in the Simulink environment so that it can be easily debugged and tuned during the test. The Ardupilot is a commercial-of-the-shelf autopilot for inner-loop control of the UAV dynamics. It is also an open source project with the onboard code available in C/C++. Hence, its function can be simulated by recompiling its source code on a virtual machine based on a standard PC. On the other hand, although it does not belong to a flight control function to be designed, the UAV dynamic model plays an important role in the SIL test, since it needs to replicate the behaviour of the real aircraft in a software environment. To this end, the X-Plane software is adopted due to its ability to simulate realistic aircraft models and flight environment like wind conditions. The three components are connected and synchronised through the TCP/IP network connection and the flight data are transferred using a dedicated protocol.

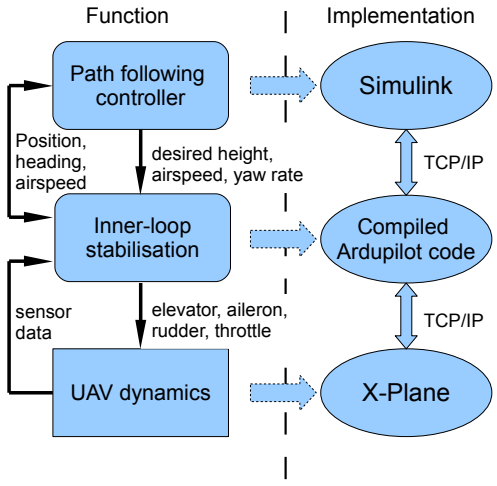

Fig. 3. Software-in-the-loop configuration

In the SIL simulation, an aircraft model with a similar dimension and power of the test UAV, which has a high fidelity of dynamics, was adopted in the X-Plane environment as the plant. The control gains in Ardupilot were then tuned to provide stabilisation for this aircraft. To mimic wind disturbances in reality, the weather condition in X-Plane was set up such that the wind was 6m/s towards north with the variances of $\pm$2m/s on the speed and $\pm$20deg on the direction.

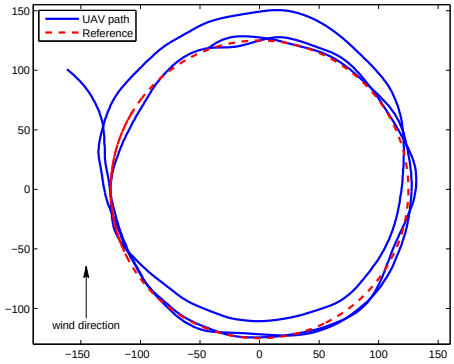

Fig. 4. SIL simulation result

One of the simulation results is presented in Fig.4. The UAV was required to follow a circle path at the airspeed of 15m/s, where the first circle was flown by the nominal control, then DOBC was switched on. It can be seen that the nominal control exhibits steady state error, whereas the proposed DOBC is able to provide accurate path following in spite of the varying wind disturbances. In addition to evaluate the performance of the proposed algorithm, the SIL simulation also verifies the integration of the high-level algorithm and the inner-loop autopilot control. This process helps to find out the potential software faults and mitigates the risk of applying the new algorithm on real UAV platform.

C. Flight experiment

After the proposed algorithm has been tested thoroughly in simulations, it can be applied on the test UAV equipped with the Ardupilot hardware. In the flight experiment the proposed algorithm is located on a ground station and is implemented in Simulink with a sampling rate of 30Hz. The ground station is equipped with the ZigBee communication module connecting to the Ardupilot, so that the real-time fight data can be transferred back to ground station and control commands can be sent to Ardupilot. The flight experiment configuration is shown in Fig.5

Initial fight tests have been conducted with some promising results. Flight test results of using the nominal control and the DOBC are given in Fig.6 and 7, respectively, which are collected from the same test flight. The wind conditions during testing were southerly at approximately 5m/s, whose influence can be observed from Fig.6. In the flight test the DOBC was turned on after 100s, and its performance can be seen from Fig.7 where the path following accuracy was massively improved. However, there also shows oscillations on the path when the UAV flew into wind. This is because the light airframe and limited power of the test UAV and it can be alleviated by further tuning the inner-loop controller in the future flight test.

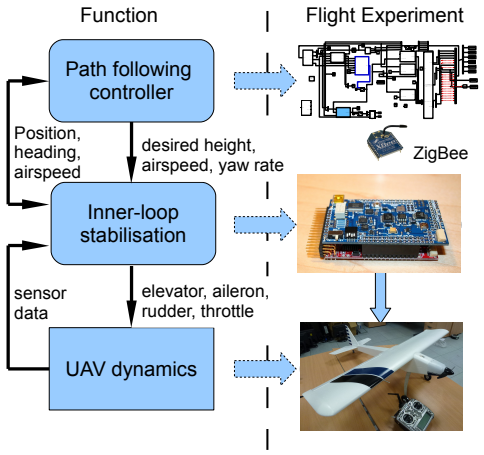

Fig. 5. Flight experiment configuration

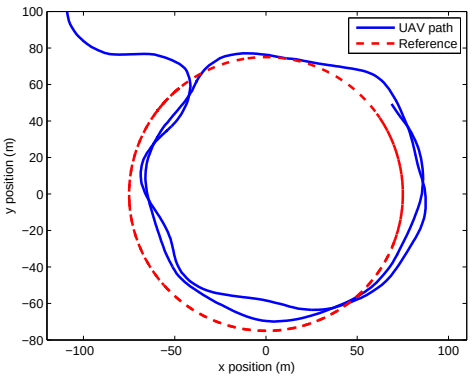

Fig. 6. Flight experiment without DOBC

V. Summary

This paper describes a disturbance observer based design of a path following controller for small UAVs in the presence of wind. The proposed controller incorporates the wind estimates into the nominal path following controller in an intuitive way such that the UAV flies into wind with a trimming angle to cancel the wind component perpendicular to the path. The formulated composite controller including the disturbance observer is proven to be globally asymptotically stable in the theoretical analysis. Its performance is evaluated in the simulation against some other control strategies and is shown to be effective. The SIL simulation is then carried out to verify its function in a more realistic environment. The initial flight experiment is also performed and some promising results are obtained. Future work following the proposed approach include the extension to 3-D case and the incorporation of UAV's lateral dynamics.

Acknowledgment

This work is supported by UK Engineering and Physical Science Research Council (EPSRC) under the Grant EP/J011525/1.

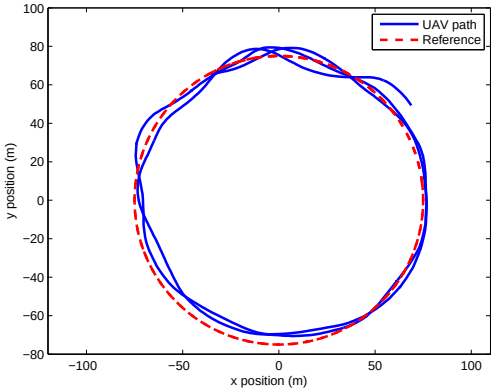

Fig. 7. Flight experiment using DOBC

References

[1] P. Encarnacao and A. Pascoal, "Combined trajectory tracking and path following: an application to the coordinated control of autonomous marine craft," in *Decision and Control, 2001. Proceedings of the 40th IEEE Conference on*, vol. 1, 2001, pp. 964 –969 vol.1.

[2] A. Aguiar, J. Hespanha, and P. Kokotovic, "Path-following for non-minimum phase systems removes performance limitations," *Automatic Control, IEEE Transactions on*, vol. 50, no. 2, pp. 234 – 239, feb. 2005.

[3] D. Soetanto, L. Lapierre, and A. Pascoal, "Adaptive, non-singular path-following control of dynamic wheeled robots," in *Decision and Control, 2003. Proceedings. 42nd IEEE Conference on*, vol. 2, Dec. 2003, pp. 1765 – 1770.

[4] I. Kaminer, A. Pascoal, E. Xargay, N. Hovakimyan, and V. Dobrokhodov, "Path following for unmanned aerial vehicles using l1 adaptive augmentation of commercial autopilots," *Journal of guidance, control, and dynamics*, vol. 33, no. 2, pp. 550–564, 2010.

[5] I. Kaminer, O. Yakimenko, A. Pascoal, and R. Ghabcheloo, "Path generation, path following and coordinated control for time critical missions of multiple uavs," in *American Control Conference, 2006*, June 2006, pp. 4906 –4913.

[6] D. Nelson, D. Barber, T. McLain, and R. Beard, "Vector field path following for miniature air vehicles," *Robotics, IEEE Transactions on*, vol. 23, no. 3, pp. 519 –529, june 2007.

[7] J. Osborne and R. Rysdyk, "Waypoint guidance for small uavs in wind," in *Infotech@Aerospace*, Sep. 2005.

[8] T. McGee and J. Hedrick, "Path planning and control for multiple point surveillance by an unmanned aircraft in wind," in *American Control Conference, 2006*, june 2006, p. 6 pp.

[9] R. Rysdyk, "Unmanned aerial vehicle path following for target observation in wind," *Journal of guidance, control, and dynamics*, vol. 29, no. 5, pp. 1092–1100, 2006.

[10] W.-H. Chen, "Disturbance observer based control for nonlinear systems," *Mechatronics, IEEE/ASME Transactions on*, vol. 9, no. 4, pp. 706 –710, dec. 2004.

[11] C. Liu, W.-H. Chen, and J. Andrews, "Tracking control of small-scale helicopters using explicit nonlinear mpc augmented with disturbance observers," *Control Engineering Practice*, vol. 20, no. 3, pp. 258 – 268, 2012.

[12] E. Panteley and A. Loria, "On global uniform asymptotic stability of nonlinear time-varying systems in cascade," *Systems & Control Letters*, vol. 33, no. 2, pp. 131 – 138, 1998.

[13] E. Frew, T. McGee, Z. Kim, X. Xiao, S. Jackson, M. Morimoto, S. Rathinam, J. Padial, and R. Sengupta, "Vision-based road-following using a small autonomous aircraft," in *Aerospace Conference, 2004. Proceedings. 2004 IEEE*, vol. 5, march 2004, pp. 3006 – 3015 Vol.5.

[14] S. Bayraktar, G. Fainekos, and G. Pappas, "Experimental cooperative control of fixed-wing unmanned aerial vehicles," in *Decision and Control, 2004. CDC. 43rd IEEE Conference on*, vol. 4, dec. 2004, pp. 4292 – 4298 Vol.4.